A novel coupling method for unresolved CFD-DEM modeling

International Journal of Heat and Mass Transfer 203 (2023) 123817

Contents lists available at ScienceDirect

International Journal of Heat and Mass Transfer

journal homepage: www.elsevier.com/locate/hmt

A novel coupling method for unresolved CFD-DEM modeling

Jingyuan Zhang [a,*], Tian Li [a,b], Henrik Ström [c], Boyao Wang [a], Terese Løvås [a]

[a] Department of Energy and Process Engineering, Faculty of Engineering, NTNU — Norwegian University of Science and Technology, Trondheim, Norway
[b] RISE Fire Research, Tiller, Norway
[c] Division of Fluid Dynamics, Department of Mechanics and Maritime Sciences, Chalmers University of Technology, Gothenburg SE-412 96, Sweden

ARTICLE INFO

Article history:
Received 20 September 2022
Revised 5 December 2022
Accepted 26 December 2022
Available online 7 January 2023

Keywords:
CFD
Forced convection
Fixed bed
Coupling
DEM

ABSTRACT

In CFD-DEM (computational fluid dynamics-discrete element method) simulations particles are considered Lagrangian point particles. The details of the flow near the particle surface are therefore not fully resolved. When the particle scale is larger than the resolved flow scale, the coupling between the CFD model and the DEM model is critical. An effective coupling scheme should minimize the risk of artificial influences on the results from choices of numerical parameters in implementations and consider efficiency and robustness. In this work, a novel coupling method is developed. The method includes both the smoothing of the particle data and the sampling of the gas phase quantities. The smoothing employs the diffusion-based method. The gas sampling method can reconstruct the filtered fluid quantities at the particle center. The sampling method is developed based on the diffusion-based method with higher efficiency. The new method avoids mesh searching and it can be easily implemented in parallel computing. The developed method is validated by the simulation of a forced convection experiment for a fixed bed with steel spheres. With the well-posed grid-independent coupling scheme, the simulation results are in good agreement with the experimental measurements. The coupling effects and the computational cost are discussed in detail.

1. Introduction

The Eulerian-Lagrangian framework is widely used to simulate multiphase systems such as particle-laden flows, evaporation processes, or pipe flows [1–3]. In the computational fluid dynamics-discrete element method (CFD-DEM) simulations of a gas-solid system, the fluid described by the Navier–Stokes equations as a continuum is resolved by the CFD solver, while the particles modeled as the dispersed phase are resolved by the DEM solver. Regarding the DEM, the particles have certain geometry information, such as size and shape, which is necessary to compute the inter-particle collisions. However, in the gas phase governing equations, the particles are represented as Lagrangian point particles (LPPs), which means the particles do not impose any physical boundary conditions at the interphase between the gas and solid phase. Simulations carried out under the LPP approach are therefore regarded as unresolved simulations in contrast to resolved particle simulations in which the details of the flow around the particle's surface are fully resolved [4], as the type A and type B particles are illustrated in Fig. 1. Unresolved CFD-DEM has widely been applied to granular flow simulations due to the much lower computational cost than the resolved simulations [5,6]. It is also an effective tool to conduct transient simulations of the thermal conversion of e.g. biomass in lab-scale fixed-bed stoves [7,8] and fluidized bed reactors [9,10].

The Eulerian and Lagrangian models are constructed using mathematical descriptions at different scales that are independent of each other. The coupling between the two models could be critical depending on the simulated situation. The point particle assumption is satisfied when the particle scale is much smaller than the resolved fluid scale. One such example is the transport of solid particles smaller than the Kolmogorov scales in a turbulent fluid flow. The coupling can be accomplished within one grid cell. The model is more reliable because the boundary conditions required by the particle sub-models can be calculated directly by interpolating or averaging from the Eulerian grid points, and the particle's feedback to the gas phase is unlikely to cause a severe disturbance. However, when the particle size is large, as the group C particles shown in Fig. 1, the coupling is not straightforward anymore. Firstly, the calculation of the local void fraction, namely the bed voidage in a fixed bed or fluidized bed, will be complicated. If the particle volume is larger than the Eulerian cell, it will induce discontinuity in the fluid. The phase volume fraction field will not change smoothly with large particles, which will cause unphysical

* Corresponding author.
E-mail address: jingyuan.zhang@ntnu.no (J. Zhang).

https://doi.org/10.1016/j.ijheatmasstransfer.2022.123817

Nomenclature

m	mass (kg)
$\mathbf{U}$	velocity (m/s)
t	time (s)
$\mathbf{F}$	force (N)
I	moment of inertia (kg/m^2)
$\mathbf{M}$	torque (N/m)
V	volume (m^3)
d_p	particle diameter (m)
C_d	drag force coefficient (-)
C_p	specific heat capacity $(J/(kg \cdot K))$
T	temperature (K)
f	view factor (-)
h_c	convective heat transfer coefficient $(W/(m^2 \cdot K))$
h_k	conductive heat transfer coefficient (W/K)
A	surface area (m^2), matrix (-)
B	matrix (-)
r	radius (m); ratio (-)
d	distance (m)
D	diffusion coefficient (m^2/s)
X	dimensionless length (-)
t^*	dimensionless time (-)
L_p	length (m)
$\mathbf{g}$	gravity (m/s^2)
h	entropy (J)
K	kinetic energy (J)
p	pressure (Pa)
S_m	mass source term $(kg/(m^3 \cdot s))$
$S_\mathbf{U}$	momentum source term $(kg/(m^2 \cdot s^2))$
b	bandwidth (m); vector (-)
Re	Reynolds number (-)
Nu	Nusselt number (-)
Pr	Prandtl number (-)
α	thermal diffusivity (m^2/s)
β	drag coefficient (-)
ϵ	emissivity (W/m^2)
ε	void fraction (-)
σ	Stefan–Boltzmann constant $(W/(m^2 \cdot K^4))$; deviation (m)
ρ	density (kg/m^3)
ω	angular velocity (s^{-1})
ϕ	passive scalar (-)
μ	viscosity $(Pa \cdot s)$
τ	diffusion time (s)
θ	dimensionless temperature (-)
p	particle
s	solid
f	fluid
r	reference
m, n	particle index;
i, j	particle index; cell index
eff	effective

fluctuations in the pressure equation [11]. This will impair the numerical stability of the CFD solver. Secondly, when the particles are viewed as points to the fluid, point particle correlations have to be used to calculate the interphase transfers, for example, the drag force correlations used to calculate the momentum exchange and the expressions of the effective heat transfer coefficients used to calculate the heat exchange. These interphase interactions, modeled with correlations, will bring two challenges. One is that the correlations require the flow quantities to be sampled from a region that is even larger than the particle scale or at the particle

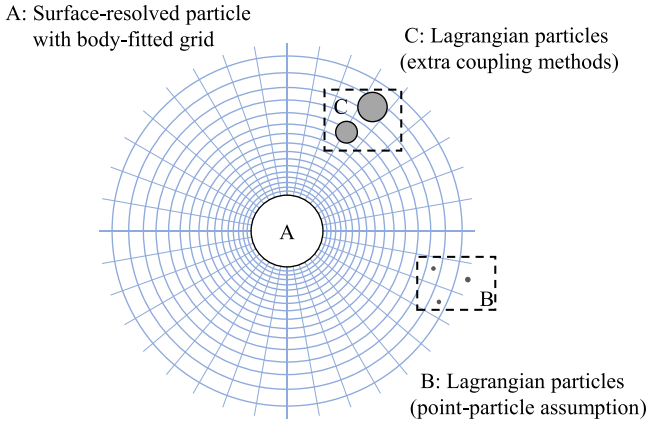

Fig. 1. Scenarios of the coupling calculation between the gas phase and the particles.

center, but without the disturbance from the particle. The other is that the interphase interactions must be projected back onto the fluid appropriately as source or sink terms to the fluid governing equations at the particle's surrounding grid cells [12]. One example of such a flow situation is the thermochemical conversion of solid fuel particles in a fixed-bed reactor, where the resolution of the temperature gradient at the conversion front generally requires a cell spacing finer than the particle size. The coupling method for calculating average gas temperature and the source term for each cell needs to be carefully designed; otherwise, the simulation will present unphysical results.

Plenty of studies have been conducted to investigate large particle coupling in unresolved CFD-DEM simulations. One strategy has been to reduce the particle's disturbance by reconstructing the undisturbed flow at the particle's location [12–14]. Ireland et al. [15] developed an analytical drag correction that improved the particle drag predictions for two-way or four-way coupled particle-fluid systems. Balachandar et al. [12] formulated an explicit expression for the particle's self-induced velocity disturbance and reconstructed the undisturbed flow velocity in order to calculate the fluid-to-particle forces. Liu et al. [13] followed Balachandar's work and developed an analogous correction procedure for self-induced temperature change by the particle. The analytical solution used to develop the corrections has some critical limitations; for example, the gas should be incompressible, and the particle is treated as a thermally thin particle. Both these assumptions would not be valid in many well-known physical processes [16]. Another strategy is to enlarge the coupling scale and smooth the coupling effects, which means smearing the coupled properties to a larger region. Capecelatro and Desjardins [6] formulated volume-filtered equations for the Eulerian-Lagrangian framework. The interactions between the particle and the fluid are considered at the characteristic length of the filtering kernel function. This method will achieve good grid independence by nature. In their work, they also proposed diffusion-based smoothing, which is an efficient method to smooth the particle quantities with a Gaussian shaped distribution. Sun and Xiao [29] and Wu et al. [1] further discussed the relationship between the diffusion-based smoothing and the Gaussian kernel distribution in a more detailed mathematical manner. Compared to other common methods for coupling large particles, such as the divided particle volume method [17,18] and the statistical kernel method [19], the diffusion-based method has advantages in computational efficiency and is easy to implement numerically. However, the studies of this method mainly focused on numerical stability and robustness by smoothing the discrete particle data. Our previous works [7,20] further developed this method and studied its implementation in the simulations of biomass combustion

processes. The inter-phase heat and mass transfers are calculated with smoothed source terms. How the Eulerian fields calculated with the smoothed particle data will further influence the coupling between the gas phase and solid phase models requires more investigation.

In this work, we propose a novel coupling method to further develop the diffusion-based method. The method uses diffusion-based filtering combined with a diffusion-based smearing method for the particle and interphase properties. The filtered gas-phase properties can be obtained at the particle's location in the CFD simulation of a dense particle system. The filtering approach avoids mesh searching and is thus efficient in parallel computing. The proposed method is implemented into a CFD solver and validated against a forced convective heat transfer experiment in a structured packed bed with steel spheres. The coupling effects in the particle heat transfer with its ambient gas phase are discussed, as well is the computational efficiency demonstrated.

2. Numerical model

2.1. CFD governing equations

The governing equations for the gas phase are the continuity, momentum and energy conservation equations of the flow and are expressed as follow:

$$\frac{\partial}{\partial t}\left(\varepsilon\rho_f\right)+\nabla\cdot\left(\varepsilon\rho_f\mathbf{U}_f\right)=0, \tag{1}$$

$$\frac{\partial}{\partial t}\left(\varepsilon\rho_f\mathbf{U}_f\right)+\nabla\cdot\left(\varepsilon\rho_f\mathbf{U}_f\mathbf{U}_f\right)=\varepsilon\mu_f\nabla^2\mathbf{U}_f-\varepsilon\nabla p+\varepsilon\rho_f\mathbf{g}+S_m, \tag{2}$$

$$\begin{aligned}&\frac{\partial}{\partial t}\left(\varepsilon\rho_f\left(h_f+K_f\right)\right)+\nabla\cdot\left(\varepsilon\rho_f\mathbf{U}_f\left(h_f+K_f\right)\right)-\nabla\cdot\left(\varepsilon\alpha_f\nabla h_f\right)\\&=\varepsilon\nabla p+\varepsilon\rho_f\mathbf{U}_f\cdot\mathbf{g}+S_h,\end{aligned} \tag{3}$$

where, ε is the void fraction. ρ_f, $\mathbf{U}_f$, μ_f, h_f, K_f and α_f are the density, velocity vector, viscosity, enthalpy, kinetic energy of the fluid phase and the effective thermal diffusivity, respectively. p and $\mathbf{g}$ are pressure and the gravity acceleration. S_m and S_h are the source terms due to the interphase momentum and heat transfer.

2.2. DEM equations

2.2.1. Particle motion model

The particle movement state is calculated under Newton's laws of motion:

$$m_i\frac{d\mathbf{U}_{p,i}}{dt}=\sum_{j=1}^{n}\mathbf{F}_{ij}^{c}+\mathbf{F}_i^{g}+\mathbf{F}_i^{f} \tag{4}$$

$$I_i\frac{d\omega_{p,i}}{dt}=\sum_{j=1}^{n}\mathbf{M}_{ij} \tag{5}$$

where, m_i, $\mathbf{U}_i^p$, I_i and ω_i^p are the mass, velocity, moment of inertia and angular velocity of the ith particle, respectively. $\mathbf{F}_{ij}^c$ and $\mathbf{M}_{ij}$ are the contact force and torque acting on the ith particle by the jth particle. n is the number of total contacts for the ith particle. The soft-sphere collision model is implemented to calculate the contact force and torque. Further details can be found in Fernandes et al. [21]. $\mathbf{F}_i^g$ is the gravity force acting on the ith particle. $\mathbf{F}_i^f$ is the particle-fluid interaction force acting on the ith particle. The drag force usually is the dominating force, and in this study, only the drag force is considered as the interaction force, which can be expressed as:

$$\mathbf{F}_i^f=\frac{V_{p,i}\beta}{1-\varepsilon}\left(\mathbf{U}^f-\mathbf{U}_i^p\right), \tag{6}$$

where, $V_{p,i}$, is the volume of the ith particle, and β is the drag coefficient. The Gidaspow model [22] is adopted to calculate the drag coefficient:

$$\beta=\begin{cases}150\frac{(1-\varepsilon)^2}{\varepsilon}\frac{\mu_f}{d_{p,i}^2}+1.75\rho_f\frac{1-\varepsilon}{d_{p,i}}\left|\mathbf{U}_f-\mathbf{U}_{p,i}\right|, & \varepsilon\leqslant 0.8\\ 0.75C_d\frac{\varepsilon(1-\varepsilon)}{d_p}\rho_f\left|\mathbf{U}_f-\mathbf{U}_{p,i}\right|\varepsilon^{-2.65}, & \varepsilon>0.8\end{cases} \tag{7}$$

where μ_f is the fluid viscosity and $d_{p,i}$ is the diameter of the ith particle. The coefficient C_d is a function of the particle Reynolds number, Re_p, given by:

$$C_d=\begin{cases}\frac{24}{Re_p}\left(1+0.15Re_p^{0.687}\right), & \text{if } Re_p\leq 1000\\ 0.44, & \text{if } Re_p>1000\end{cases} \tag{8}$$

$$Re_p=\frac{\varepsilon\rho_f\left|\mathbf{U}_f-\mathbf{U}_p\right|d_p}{\mu_f}. \tag{9}$$

2.2.2. Particle heat transfer model

The particle will exchange heat with its surrounding through convection, conduction and radiation. The heat balance equation of the particle is formulated as:

$$\begin{aligned}m_iC_{pp,i}\frac{\mathrm{d}T_{p,i}}{\mathrm{d}t}&=\epsilon\sigma f\left(T_{eq,i}^4-T_{p,i}^4\right)+\sum_{j=1}^{n}h_{k,ij}\left(T_{p,j}-T_{p,i}\right)\\&\quad+h_{c,i}A_{p,i}\left(T_f-T_{p,i}\right),\end{aligned} \tag{10}$$

where $C_{pp,i}$, $T_{p,i}$, $A_{p,i}$ are the heat capacity, surface temperature and surface area of the ith particle, respectively. ϵ, σ and f are the emissivity, the Stefan–Boltzmann constant and the view factor. The radiation control volume method is applied to simplify the calculation for the radiation model [23]. $T_{eq,i}^4$ is the ith particle's ambient equivalent radiation temperature which is calculated as follows:

$${T_{eq,i}}^4=\varepsilon T_f^4+(1-\varepsilon)\frac{1}{m}\sum_{j=1}^{m}{T_{p,j}}^4. \tag{11}$$

m is the neighboring particle number in the ith particle's radiation control volume. Unlike Mehrabian's implementation [23], the quartic average is used to calculate the equivalent radiation temperature. To avoid a massive particle searching procedure, which is carried out to determine m, the neighboring particles are represented by the direct contacting particles ($m=n$, n being the same as in Eq. (4)). The view factor is assumed to be 1. Since the simulations in this work are carried out in a stagnate packed bed and all the particles' temperatures are largely below 823K [24], the heat conduction and radiation between the particles are not expected to have a significant contribution to the heat transfer. The above simplifications will not cause notable influence. For high-temperature cases, when the radiation heat transfer becomes significant, more detailed radiation models need to be considered [25].

The heat conduction between the contacting particles can be calculated together with the collision model. According to the soft-sphere collision model's assumption, particles are allowed overlap. Batchelor and O'brien [26] proposed a method to calculate the contacting heat conduction, and a modified version by Zhou et al. [27] is adopted in this work. The equivalent conduction heat transfer coefficient between the ith and jth particle, $h_{k,ij}$ can be calculated as:

$$h_{k,ij}=\frac{4r_{c,ij}}{\left(1/k_{p,i}+1/k_{p,j}\right)}, \tag{12}$$

where k_p is the particle's thermal conductivity. $r_{c,ij}$ is the contacting radius of the overlapping circle and can be resolved from Heron's formula, which is calculated as:

$$r_{c,ij} = \frac{2A}{d_{ij}}, \tag{13}$$

$$A = \sqrt{s(s-r_j)(s-r_i)(s-d_{ij})}, \tag{14}$$

$$s = \frac{(r_j + r_i + d_{ij})}{2}, \tag{15}$$

where r_j and r_i are the radius of particles j and i, respectively, and d_{ij} is the distance between the centroids of particles j and i.

As for heat convection, there are various choices of correlation of heat transfer coefficient. A widely used correlation for particles in fixed beds was proposed by Wakao and Kagei [28] as follows:

$$Nu_p = 2 + 1.1 Pr_f^{1/3} Re_p^{0.6}, \tag{16}$$

where, Nu_p is the particle Nusselt number, and Pr_f is the Prandtl number of the fluid.

The simulated case in this work is a forced convection case, and the heat transfer coefficient will play an important role. Wakao's equation does not include the influence of the bed voidage in an explicit way. In another simulation of the same experimental case as in this work, the correlation recommended by KTA 3102.2 standard [1] is adopted as shown in Eq. (17):

$$Nu_p = 0.33 Pr_f^{0.5} Re_p^{0.86} \varepsilon^{-1.07} + 1.27 Pr_f^{1/3} Re_p^{0.36} \varepsilon^{-1.88}. \tag{17}$$

For the simulated case, the heat transfer coefficient was also measured by experimental fitting. The choice of different coefficients, either by using experimental fitting or using correlations, will be compared and discussed in later sections.

3. Interphase coupling

Spatially extending the interphase coupling will smooth the changing of the quantities of the fluid phase and reduce the disturbance introduced by the particles. On a practical level, the coupling includes two aspects. The first is to find proper kernel functions to redistribute and smooth the particle quantities present in the CFD governing equations, rather than couple them back to the fluid by a Dirac delta function shaped distribution. The second is to transfer the gas phase properties present at the Eulerian grid points into the 0D data required by the particle sub-models. In this work, both the smearing method for the particle data and the sampling method for the fluid data are applied based on a Gaussian distribution. The solver is developed using the open-source software OpenFOAM®7, and the code is publicly available at https://github.com/ComKinBio/fixedBedHeatTransFilteredFoam under GPLv3 license.

3.1. Diffusion based smoothing

Diffusion-based smoothing is a widely used method for smearing the particle data [6,29,30]. For any particle quantity (including the source/sink terms generated by the particle sub-models), the quantity is initialized to a discrete field or a mollified field [6], which is presented in the Eulerian mesh based on the particles' locations. Then it is resolved by a Laplace diffusion operator, as shown in Eq. (18):

$$\frac{\partial \phi}{\partial \tau} = D \nabla^2 \phi, \tag{18}$$

where, D is a diffusion coefficient, and τ is the diffusion time variable. In order to distinguish it from the physical time, t, τ is in this work only employed for the smoothing diffusion.

Sun and Xiao [29] and Wu et al. [1] used different mathematical methods to prove that applying the diffusion operation to a field is equal to smooth the field by a Gaussian kernel function. For example, with $\mathbf{x}$ as the 3D location vector, consider the diffusion of a variable $u(\mathbf{x}, t)$:

$$\frac{\partial}{\partial \tau} u = D \nabla^2 u. \tag{19}$$

If the distribution of u at $\tau = 0$ is given as $u(\mathbf{x}, 0)$, the distribution of u at an arbitrary τ can be calculated using the Green function:

$$u(\mathbf{x}, \tau) = \int_V G\big(\mathbf{x}, \mathbf{x}'; \tau, 0\big) u\big(\mathbf{x}', 0\big) d\mathbf{x}', \tag{20}$$

where the Green function is:

$$G\big(\mathbf{x}, \mathbf{x}'; \tau, \tau'\big) = \frac{1}{(4\pi D(\tau - \tau'))^{3/2}} e^{-\frac{\left(\mathbf{x}^T\mathbf{x} - \mathbf{x}'^T\mathbf{x}'\right)^2}{4D(\tau - \tau')}}, \tag{21}$$

while a 3D Gaussian function kernel for the particle i is:

$$g(\mathbf{x} - \mathbf{x_i}) = \frac{1}{\left(2\pi\sigma^2\right)^{3/2}} e^{-\frac{\left(\mathbf{x}^T\mathbf{x} - \mathbf{x}_i^T\mathbf{x}_i\right)}{2\sigma^2}}, \tag{22}$$

where $\mathbf{x_i}$ is ith particle center vector. It is clear that by applying the diffusion operator and having the diffusion start at $\tau = 0$, a field will be smoothed in the same way as by a Gaussian kernel function with one standard deviation of $\sigma = \sqrt{2D\tau}$. We can define σ as a characteristic length of the smoothing length scale. There is no need for special treatment of physical boundaries for the diffusion operator. Using zero gradient conditions at the boundaries of the computational domain, the diffusion operator will ensure the conservation of the diffused properties [29].

3.2. Filtering of the gas phase

To enable a mesh-independent setup when particles are no longer small in relation to the size of the computational cells, one must be able to account for the fluid information on a larger scale than that of a single mesh cell. In such situations, the locally filtered fields of the fluid data can be calculated from the point values on the Eulerian mesh by a convolutional integral. The filtered field of a gas phase quantity, $\mathbf{a}(\mathbf{x}, t)$, is computed by using the convolution product with the filtering kernel g, the same as Eq. (22) [31]:

$$\bar{\mathbf{a}}(\mathbf{x}, t) = \int_{\mathcal{V}} \mathbf{a}(\mathbf{y}, t) g(|\mathbf{x} - \mathbf{y}|) d\mathbf{y}, \tag{23}$$

where, $\mathcal{V}$ is the whole fluid domain. The filtering disregards the phase fraction by assuming the phase fraction is uniform in the densely packed bed, and this assumption is valid when the particle volume is diffused sufficiently. Analogous to the diffusion-based smoothing, the filtering operation can be achieved by using a diffusion operator if the diffusion time and the kernel length scale satisfy $\sigma = \sqrt{2D\tau}$. In Appendix A, a mathematical proof based on the discrete numerical calculation has been provided to shown that such analogous is valid. It is important to point out the difference between t and τ. At any physical time t, the $\mathbf{a}(x, t)$ field should be diffused by Eq. (18) from 0 to $\tau = \sigma^2/2D$, in order to obtain the filtered field $\bar{\mathbf{a}}(\mathbf{x}, t)$. The gas phase data required by the particle sub-models can be read directly from the cell or by interpolating to the particle centroid location from the filtered fields $\bar{\mathbf{a}}(\mathbf{x}, t)$.

In this work, we also propose another calculation scheme to get the filtered field, which has different characteristics than that outlined above. Instead of directly applying the diffusion operator on the gas property fields, the filtering kernel field for individual particles is calculated based on their location. First we initialize a new

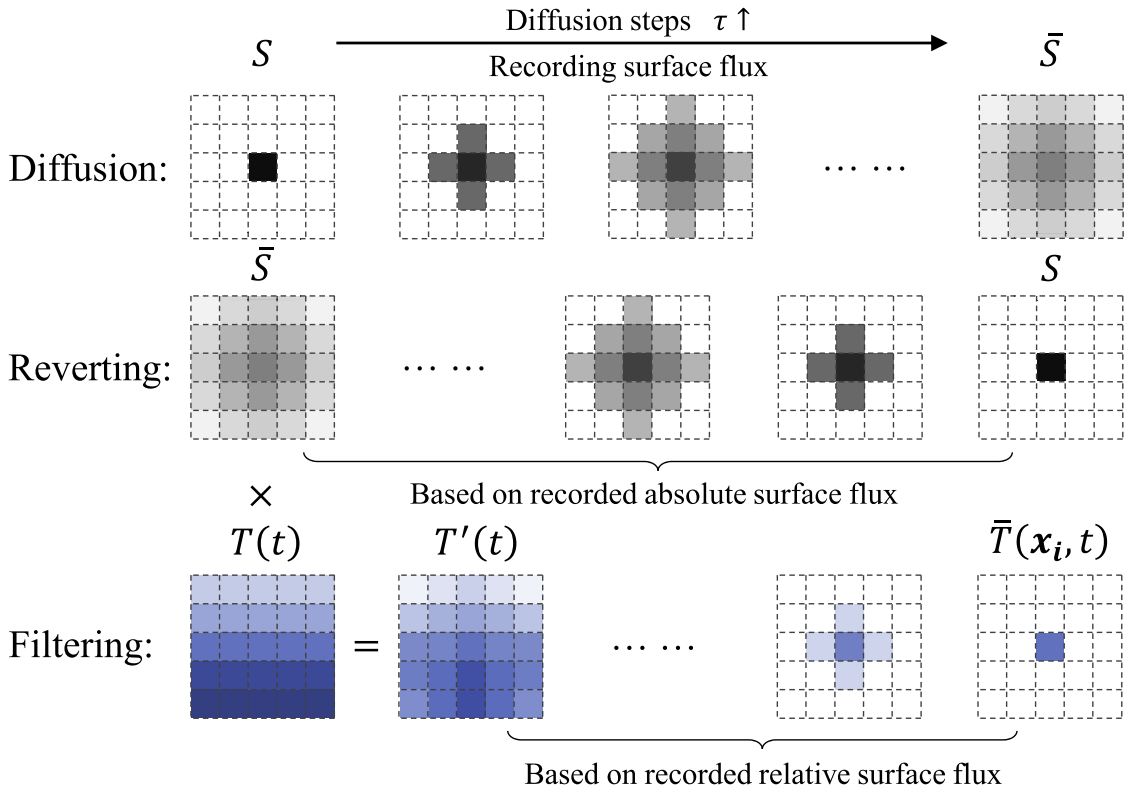

Fig. 2. Illustration of the discrete calculation of the new filtering method based on the single-particle scenario.

scalar field, S, using the Dirac delta function and the particle's location:

$$S(\mathbf{x}, t) = \sum_{i=1}^{m} \delta(\mathbf{x} - \mathbf{x_i}), \tag{24}$$

where, m is the total particle number. Then we apply the diffusion operator to S, and by applying Eqs. (20) and (21), the $\bar{S}$ field can be expressed by:

$$\bar{S}(\mathbf{x}, t) = \sum_{i=1}^{m} G(\mathbf{x} - \mathbf{x_i}; \tau, 0). \tag{25}$$

The $\bar{S}$ field is an overlay field of the filtering kernel function for every particle, and it satisfies $\int_{\mathcal{V}} \bar{S}(\mathbf{x}, t) d\mathbf{x} = m$. It can be used to take the weighted average of a gas data field for the particles. For example, multiplying $\bar{S}$ with the gas temperature field T yields a temporary field T' ($T' = \bar{S}T$), and by calculating the integral over the domain, then by combining with Eq. (23) we get:

$$\int_{\mathcal{V}} T' d\mathbf{x} = \sum_{i=1}^{m} \int_{\mathcal{V}} TG(\mathbf{x} - \mathbf{x_i}; \tau, 0) d\mathbf{x} = \sum_{i=1}^{m} \overline{T}(\mathbf{x_i}, t). \tag{26}$$

The result is the sum of the filtered T values at the particle centroids. The sum is however not as useful as the data of each $\overline{T}(\mathbf{x_i}, t)$. In fact, we can design a scheme to obtain $\overline{T}(\mathbf{x_i}, t)$ at each corresponding cell centroid, and the illustration of the discrete calculation based on the single particle is shown in Fig. 2. First, we need to resolve the diffusion of the S field with an explicit method. In every diffusion time step, the explicit method will calculate the gradient (∇S) at each cell center and calculate the divergence ($\nabla \cdot \nabla S$) by interpolating ∇S values at the cell faces from the values at cell centers. As shown in Fig. 3, the two cells that share face f_{ij} are registered as the owner cell and neighbor cell of face f_{ij}.

With the explicit method, the scalar S can only be transported between face-neighboring cells in one diffusion time step. If we record the ΔS_{ij}^{τ} transported through every mesh face in every diffusion time step, we will be able to monitor the entire diffusion process explicitly. By reversing the diffusion time step and the direction of the ΔS_{ij}^{τ} transport at the mesh faces, we can use $\bar{S}(\mathbf{x}, t)$ to reconstruct $S(\mathbf{x}, t)$. This is exactly the reverse process of the diffusion of S. However, instead of reversing the S field, it is the T' field that needs to be reversed in the coupling calculation. In order to achieve this, it is the transport ratio, $r_{ij}^{\tau+1}$, of $\Delta S_{ij}^{\tau} / S_i^{\tau+1}$ that should be recorded instead of ΔS_{ij}^{τ} (note that i is the receiver cell index of the transported S; $r_{ij}^{\tau+1}$ is positive if S is transported from the neighbor cell to the owner cell, and negative if S is transported from the owner cell to the neighbor cell). The reversing process is simply looping r_{ij} at every diffusion time step and mesh faces and performing the calculation of T' by the following:

$$\begin{cases} T_i'^{\tau} = T_i'^{\tau} + r_{ij}^{\tau+1} T_i'^{\tau+1}, T_j'^{\tau} = T_j'^{\tau} - r_{ij}^{\tau+1} T_i'^{\tau+1}; & \text{if } r_{ij}^{\tau+1} > 0 \\ T_i'^{\tau} = T_i'^{\tau} + r_{ij}^{\tau+1} T_j'^{\tau+1}, T_j'^{\tau} = T_j'^{\tau} - r_{ij}^{\tau+1} T_j'^{\tau+1}; & \text{if } r_{ij}^{\tau+1} < 0 \end{cases} \tag{27}$$

After the reversing process, $\overline{T}$ will be reconstructed using the $T'(\mathbf{x}, t)$ field, which now only contains the values of the cells that the particles' centroids are located in. The calculation scheme can be summarized as the following:

1. Initialize the S field using Eq. (26).
2. Apply the diffusion operator to S using an explicit method to get the $\bar{S}$ field, and record r_{ij} in a two-dimensional table (one dimension is the diffusion time step, the other is the mesh face id).
3. Calculate the T' field as $T' = \bar{S}T$.
4. Loop the diffusion time step in the reverse way, and in every diffusion time step loop r_{ij} perform the calculation of Eq. (27) in order to obtain the filtered $\overline{T}(\mathbf{x_i}, t)$ field.

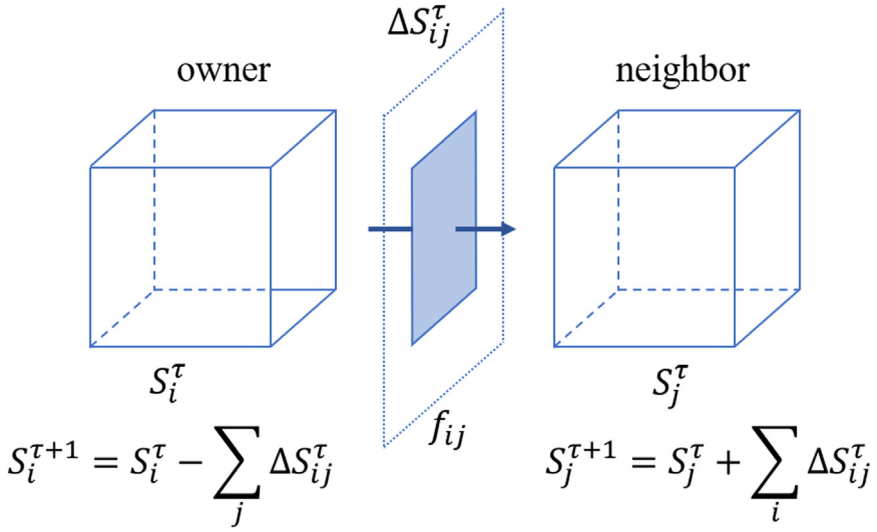

Fig. 3. Discrete scheme of the Laplacian diffusion with the explicit method.

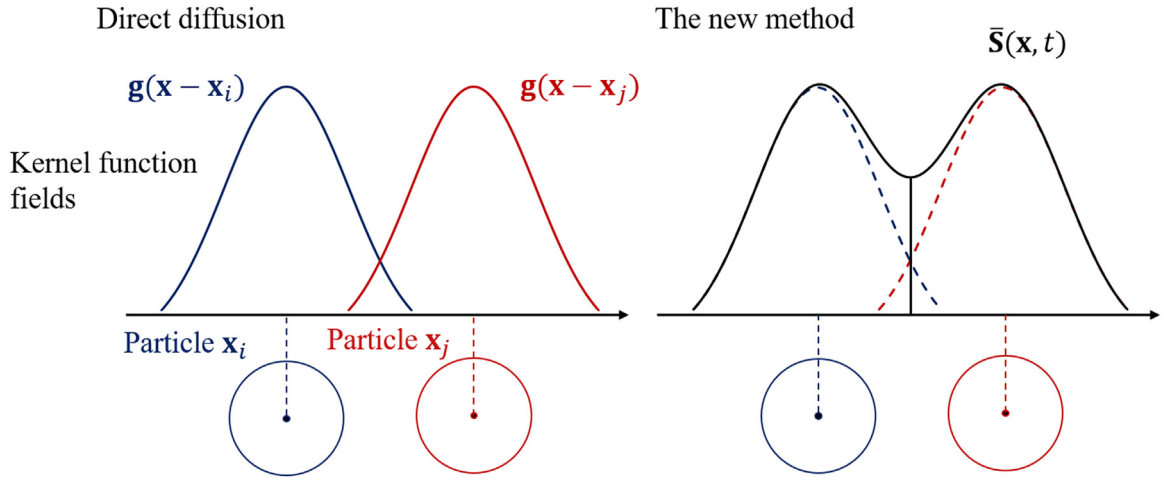

Fig. 4. The kernel function fields by different filtering methods. (The blue and red lines represent the original Gaussian kernel function, and the solid black line represents the implemented kernel function by the new method.) (For interpretation of the references to colour in this figure legend, the reader is referred to the web version of this article.)

There are three main advantages of the new filtering operation. The first is that the filtered values that are needed for the particle consideration are calculated at the cells in which the particles' centroids are located, hence the DEM code can easily access these values. The second advantage is that the particle centroid cell obtains the averaged information from the non-adjacent cells without mesh searching, which can otherwise be a computationally costly procedure. For example, in order to calculate the discrete cumulative kernel function in one cell, all the contributor cells need to be found through a mesh searching procedure. The third advantage is that all the calculations are based on the mesh faces, and there is thus no need for additional considerations for parallel computing.

Compared to directly applying Eq. (18) to obtain the filtered gas phase quantities, the new method will have different filtered values at the particle location, $\mathbf{x_i}$, even when they use the same filtering length scale. This happens when the particle is close to its neighboring particles. With multiple particles, the kernel function field, $\bar{S}(\mathbf{x}, t)$, has virtual boundaries between every two particles, as shown in Fig. 4. The diffusion of S is driven by the gradient ∇S. At the virtual boundaries, the gradient is 0, and there will be no transport through the neighboring cell face. In Fig. 4, for the new method, the shape of the kernel function will be the solid black line instead of the dashed lines. Compared to the direct diffusion method, the new method will always have a deformed Gaussian kernel with a more narrow distribution in length scale, and the consequences will be further discussed in Section 5.

4. Validation

An experiment with forced convective heat transfer in a structured packed bed [32] is simulated to validate the proposed CFD-DEM model. The bed is packed in the form of a simple cubic packing with steel spheres. The bed geometry and the corresponding computational mesh are illustrated in Fig. 5. The initial particle temperature is 338K, and cold air is used to cool the spheres, introduced at the rear inlet with an initial temperature of 298K. The thermal physical properties of the particles are listed in Table 1.

Based on the geometry, the structured mesh with a cell side length of 4mm was generated, which according to previous CFD-DEM simulations with diffusion-based smoothing, should be fine enough to resolve the gas flow [1]. To keep the Courant number smaller than 1, the fluid computational time step was set to 10^{-3}s. An adiabatic wall assumption was used in the simulation, which is reasonable considering that the temperatures in the experiments

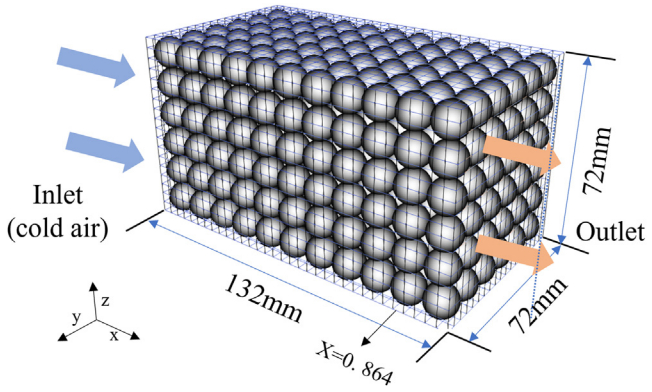

Fig. 5. The geometry of the fixed bed of cubic packing.

Table 1
Particle physical properties.

	Value	Unit	Ref.
Density	7.81×10^3	$kg \cdot m^{-3}$	[32]
Diameter	0.012	m	[32]
Thermal conductivity	40.1	$W \cdot m^{-1} \cdot K^{-1}$	[32]
Heat capacity	553.0	$J \cdot kg^{-1} \cdot K^{-1}$	[32]
Elastic modulus	10^{11}	Pa	-
Poisson's ratio	0.35	-	-

were rather low and the material of the walls was plexiglass, which has a relatively high heat resistance. As outlined above, the filtering length scale is defined as σ, and for the simulations in this section, $\sigma = d_p$. The selection of the filter length scale is further discussed in Section 5.1. For the experimental fitting of the heat transfer coefficient, we have that $Nu_p = 47.56$ [32], which was also adopted in the simulations in this section, while the studies of using different correlations for Nu will be further discussed in Section 5.2.

The new coupling method as developed in this study is employed, and two variations thereof are compared. As mentioned in Section 3, the coupling has two aspects which can be summarized as (1) sampling the gas data for the particle sub-models and (2) smoothing the particle data or interphase exchanging quantities for the gas phase governing equations. The three coupling methods all employ the diffusion-based smoothing method, which means Eq. (18) will be applied to all the particle data that need to be smoothed, but they are different in the method of *sampling*. The new method employs the calculation scheme proposed in Section 3.2 and is hereafter referred to as the diffusion-based sampling (DBS) method. This method is contrasted against three alternate approaches (two other coupling methods and the conventional CFD-DEM approach without any specific coupling method). The approach where the sampling is implemented by directly reading the grid cell values or interpolated values without the use of any filtering method is referred to as the no filtering (NF) method. The method where the sampling is achieved by directly applying Eq. (18) to obtain the filtered gas phase quantities is referred to as the direct diffusion (DD) method. In addition, the conventional CFD-DEM without any specifically designed coupling method (NONE) is also employed for comparison. The differences of all the coupling methods are summarized in Table 2.

The non-dimensional temperatures of the gas phase and the solid phase, distance and time are defined as:

$$\theta_f = \frac{T_f - T_r}{T_{p,0} - T_r}; \quad \theta_s = \frac{T_p - T_r}{T_{p,0} - T_r}; \quad X = \frac{x}{L_p}; \quad t^* = \frac{t}{L_p/\mathbf{U}_{in}}, \tag{28}$$

where T_f is the gas temperature measured at the outlet in the experiments (the mass-flow weighted temperature was used as the simulation results) and T_p is the particle's center temperature measured at selected particles close to the central line (the Biot number is about $0.03 << 1$, and the thermally thin particle model was used in the simulation, which assumes the particle is isothermal). T_r is the reference temperature (298K) and $T_{p,0}$ is the initial solid phase temperature. L_p is the length of the fixed bed (132mm). $\mathbf{U}_{in}$ is the gas phase inlet velocity ($1.23\ m/s$).

Table 2
Comparison of different coupling methods.

Method label	Gas data sampling	Particle data smoothing
NF	None	Applying diffusion equation to particle properties and source terms
DD	Applying diffusion equation to gas phase properties	Same as NF
DBS	Using calculation scheme in Section 3.2	Same as NF
NONE	None	None

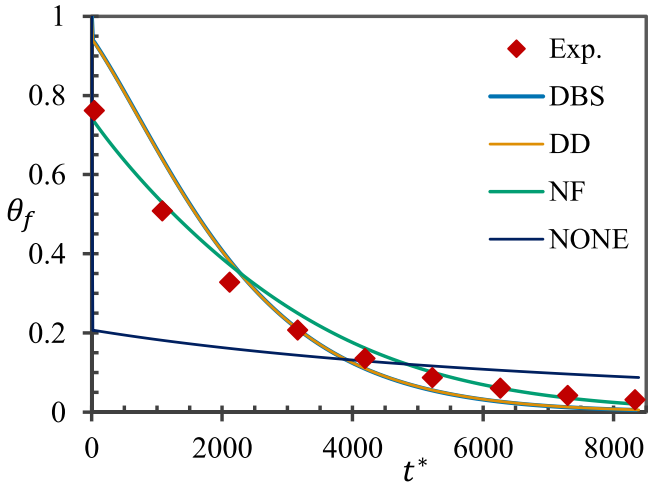

Fig. 6. Comparisons of measured and predicted gas phase outlet temperature θ_f with different coupling methods.

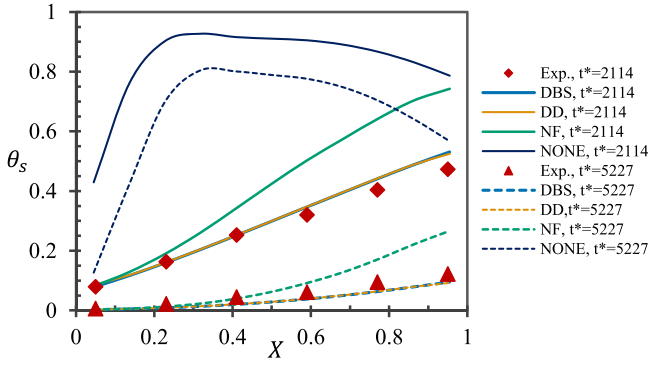

Fig. 7. Comparisons of measured and predicted solid phase temperature θ_s with different coupling methods.

As shown in Fig. 6, the predicted outlet gas phase temperature after the cooling process by using the NF method provided better agreement with the measurements than DBS and DD. There is little difference between the DD and DBS methods, which both make use of gas filtering methods. However, as shown in Fig. 7, the NF method predicted a higher particle temperature compared to the experimental measurements. The heat transfer source term S_h in Eq. (3) is smoothed by applying Eq. (18). The diffusion-based smoothing method will introduce artificial diffusion of the inter-

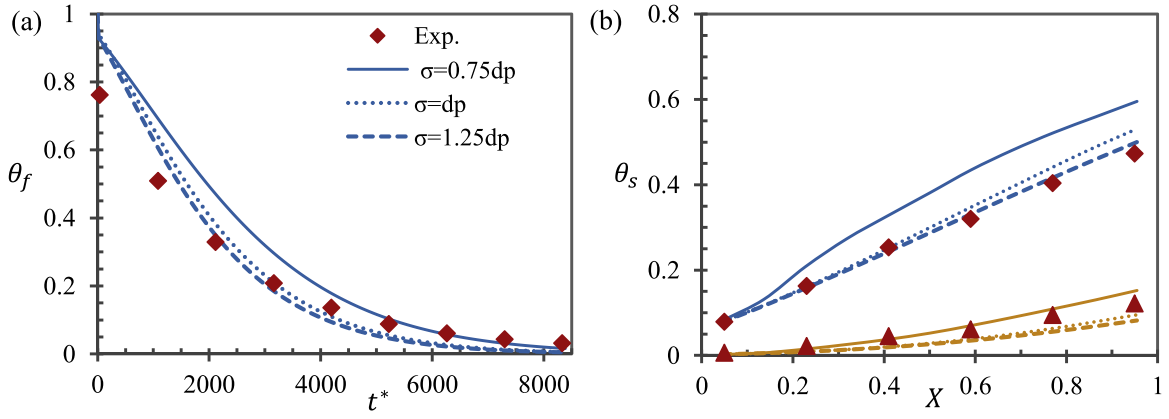

Fig. 8. Comparisons of measured and predicted temperatures of gas phases (a) and solid phases (b) with different coupling scales by DBS method. (In figure (b), the ◆ and the blue lines are the Exp. data and simulation results when $t^* = 2114$, respectively; the ▲ and the yellow lines are the Exp. data and simulation results when $t^* = 5227$, respectively.) (For interpretation of the references to colour in this figure legend, the reader is referred to the web version of this article.)

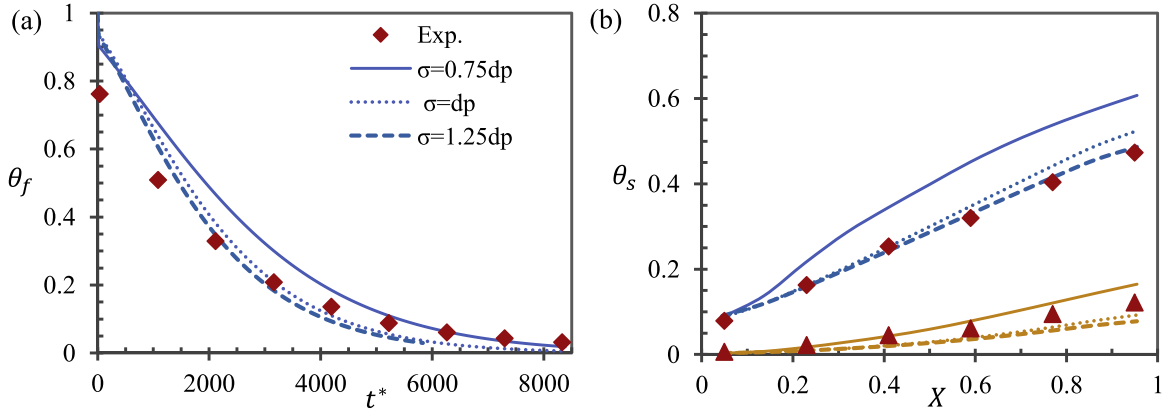

Fig. 9. Comparisons of measured and predicted temperatures of gas phases (a) and solid phases (b) with different coupling scales by DD method. (In figure (b), the ◆ and the blue lines are the Exp. data and simulation results when $t^* = 2114$, respectively; the ▲ and the yellow lines are the Exp. data and simulation results when $t^* = 5227$, respectively.) (For interpretation of the references to colour in this figure legend, the reader is referred to the web version of this article.)

phase exchanging quantities [20]. Consequently, the source term S_h is coupled back even to the upstream region of the gas flow. The source term S_h will raise the gas phase temperature, resulting mainly from convection. However, it will further influence the sampling of the gas phase temperature, which is needed for the convection calculation. For the NF method, the gas phase temperature is sampled at the particle's centroid, and the disturbance introduced by the particle to the temperature field of the gas phase has a larger influence on the coupling calculation than that in the other two methods with gas filtering. The NF method underestimated the heat transfer rate between the gas and the particles, resulting in over-prediction of the particles' temperatures.

However, the smoothing of S_h is necessary, otherwise a large source term will strongly impair the solver's robustness. For example, the simulation failed to predict a reasonable result without any filtering and smoothing method (NONE).

In general, the DD and DBS methods showed good performance compared with the experiments. The results showed that the developed filtering methods successfully reconstructed the ambient gas phase temperature seen by the particles. Since S_h is smoothed, the NF method also predicted much better results than without coupling methods. If the interphase heat exchange is not the only reason for the gas phase temperature changing, for example, if there are strong endothermic or exothermic homogeneous gas phase reactions, then the filtering methods will play a much more important role in the simulation.

5. Discussion

5.1. Length scale in diffusion and filtering

In the coupling models, the filtering and smoothing length scale is a chosen parameter. It defines the spatial scale on which the interaction between the gas and the particle takes place. Sensitivity studies of this parameter are presented in this section. Three different length scales were investigated; σ equal to $0.75d_p$, d_p and $1.25d_p$, respectively.

As shown in Figs. 8 and 9, the DD and DBS methods predicted very similar results (e.g., the relative mean differences of the gas temperature prediction based on DD are 5.18%, 0.69% and 0.67%, when σ equals $0.75d_p$, d_p and $1.25d_p$, respectively). As the length scale became larger, converged results were obtained. The major difference between the two methods is that when $\sigma = 0.75d_p$, the predicted outlet gas temperature has deviations at the early stage. That is because of the fundamental difference in the sampling methods, which is shown in Fig. 4. Due to the particle blocking effects for the smoothing of the S field, the sampling calculation will be less sensitive to the length scale for the DBS method. For both DD and DBS methods, the different predictions using different length scales are mainly influenced by the smoothing of the particle data.

However, the NF method is significantly affected by the selection of the length scale, as shown in Fig. 10. As expected, when

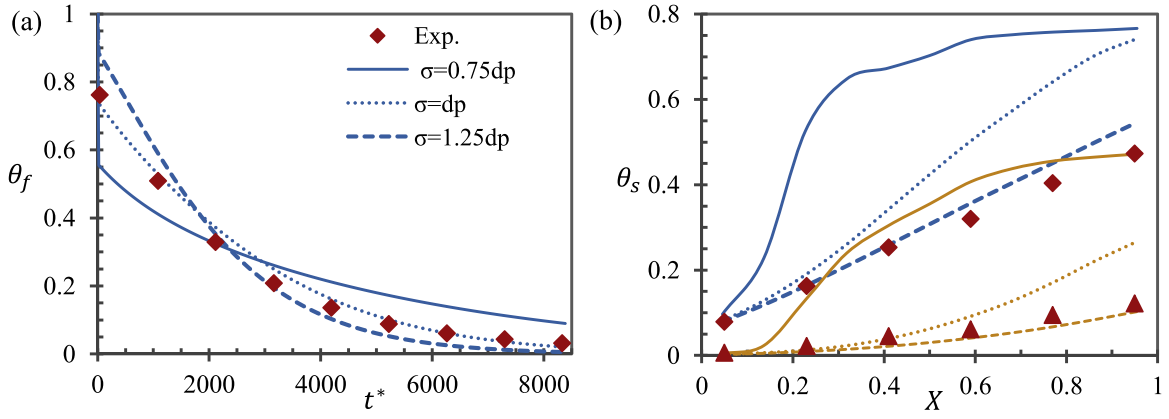

Fig. 10. Comparisons of measured and predicted temperatures of gas phases (a) and solid phases (b) with different coupling scales by NF method. (In figure (b), the ◆ and the blue lines are the Exp. data and simulation results when $t^* = 2114$, respectively; the ▲ and the yellow lines are the Exp. data and simulation results when $t^* = 5227$, respectively.) (For interpretation of the references to colour in this figure legend, the reader is referred to the web version of this article.)

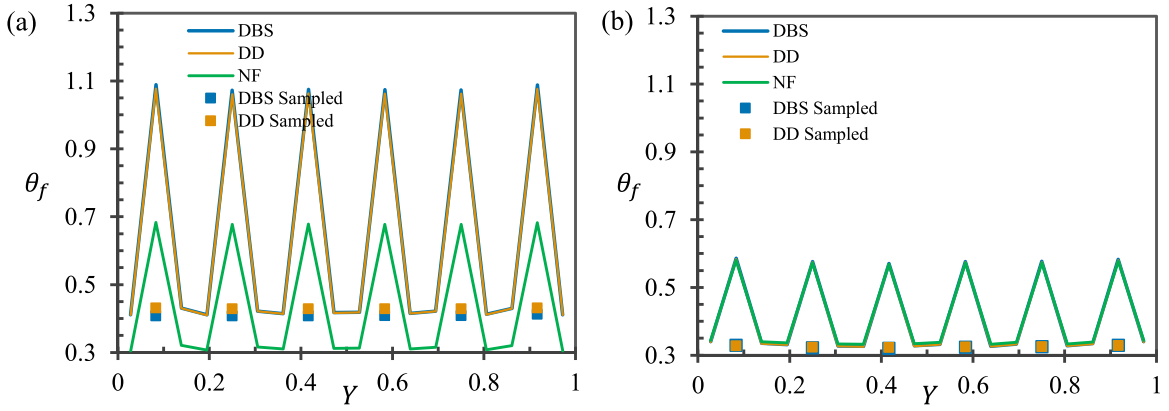

Fig. 11. Predicted and sampled temperatures of gas phases in Y direction with different coupling methods at $X = 0.864$: (a) $\sigma = 0.75d_p$; (b) $\sigma = d_p$.

σ becomes smaller, the behavior of the NF method will get closer to that of the conventional CFD-DEM method, which is shown as NONE in Figs. 6 and 7. When σ becomes larger, the NF method will be closer to the DD and DBS methods. Since the heat source term is already smoothed to a certain degree, the gas filtering methods hardly further influence the gas data sampling.

The above results show that the gas filtering methods are essential when the particle data is not fully smoothed. At the same time, gas filtering methods are not sensitive to the length scale, as long as the length scale is large enough. As the length scale is defined using the deviation of the normal distribution, 20% of values are distributed within one deviation away from the particle centroid and about 73% of the values are distributed within two standard deviations [33]. The length scale is defined differently in studies that employed the diffusion-based method. For example, Sun and Xiao [29] defined the length scale as the bandwidth, $b = \sqrt{2}\sigma$, and Capecelatro and Desjardins [6] defined the length scale as $\delta_{\frac{1}{2}}$, which is the full width at half the height of the kernel function. In the above research, the length scale is recommended to employ a value of $3d_p - 6d_p$. However, it is worth noting that the above two studies were conducted in 1D or 2D. The 3D normal distribution has a lower probability within the same deviation range than in 1D or 2D. From this study, when $\sigma > d_p$, it can be regarded as large enough for the coupling with the gas filtering method.

The gas phase temperature at location $X = 0.864$ is plotted along the y direction in Fig. 11. There are six particles arrayed in the y direction. The solid lines are the gas phase temperature profiles, and the marks are the particles surrounding gas phase temperatures sampled by the gas filtering methods. When $\sigma = 0.75d_p$, the heat transfer source term has a more concentrated distribution at the cell where the particle's centroid is located, and this uneven distribution developed more strongly as the flow developed. This disturbance to the gas temperature field introduced by the particle further influenced the calculation of the source term of the interphase heat transfer in the NF method. The DBS and the DD methods reconstructed the particle ambient temperature, and the coupling effects from the diffusion-based method had, however, less influence on the calculation of the convection, as shown in Figs. 8 and 9.

The smoothing procedure of the S field in the DBS method is illustrated in Fig. 12. The $\bar{S}$ field ended up with a very even distribution by the given length scale. Since the S field is determined by the particle number, unlike the DD method, the filtered gas property fields will contain the discrete values at the cells where the particle's centroid is located, e.g., the temperature field (T) shown in Fig. 13. One disadvantage of the DBS method is that the sampling centroid is the cell's centroid rather than the particle's centroid and interpolation schemes are not applicable. However, the DBS method is designed for the situation where the particle size is much larger than the grid size, and this disadvantage can be neglected.

As mentioned in Section 3.2, the diffusion calculation of the S field is meaningless when $\nabla S = 0$. In this study, the passive scalar S will only be transported to the 26 neighboring cells from the particle center cell with the simple cubic packed particles. As mentioned above, the particle blocking effects will restrict the sampling calculation for one particle within the 27 cells that make up the cubic space with the side length of d_p. However, for the DD

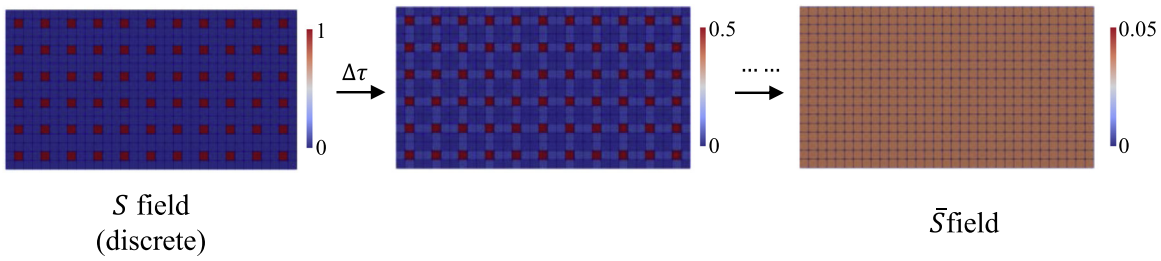

Fig. 12. The smoothing of the S field in the DBS method, $\sigma = 1.25d_p$.

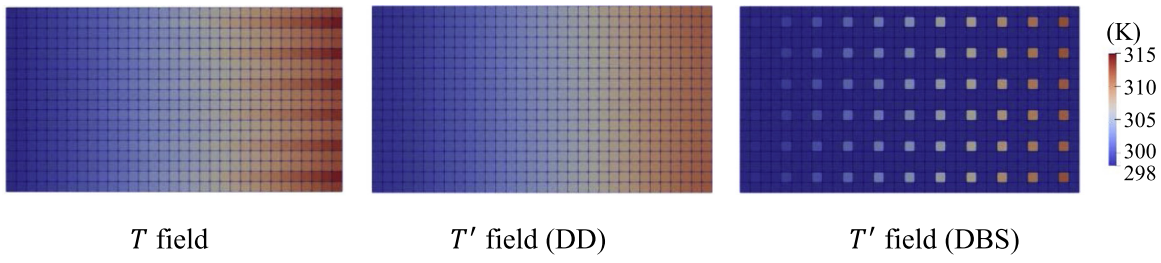

Fig. 13. Predicted and sampled temperatures of gas phases by different coupling methods, $\sigma = 1.25d_p$.

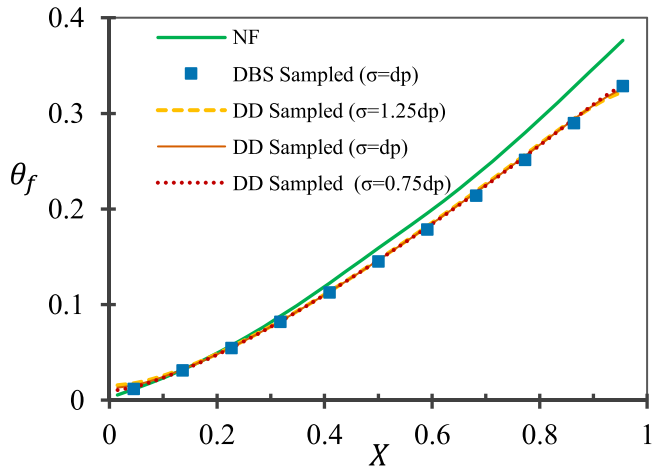

Fig. 14. Predicted temperatures of gas phases in x direction with different coupling methods.

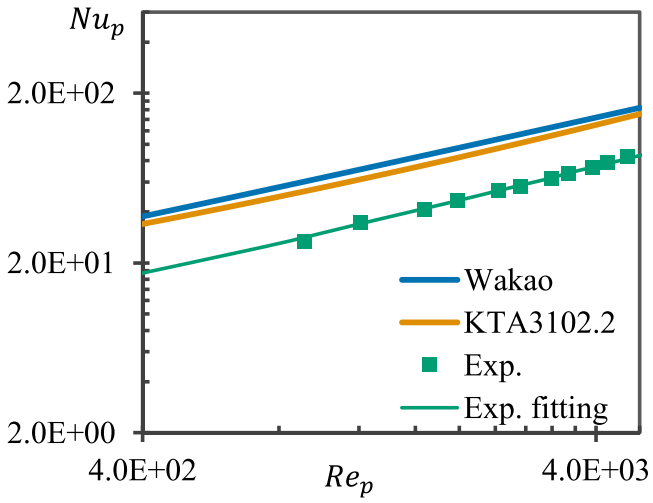

Fig. 15. Measured and predicted particle Nu numbers with different correlations.

method, as the length scale increases, the T' will converge to a uniform distribution. Fig. 14 shows the sampled temperature by using the DBS and DD methods, respectively, which is based on the gas temperature profile in the x direction predicted by the NF method at $t^* = 2114$. There is no observable difference for the DBS method by using different σ, so only the result with $\sigma = d_p$ is shown. For the DD method, there are slight differences between the sampled temperature with different σ.

The above results show that the smoothing process provides the solver with more robust and accurate capabilities. The gas filtering method is also critical to the consistency of the coupling calculation. The DBS and DD methods are developed from the same Gaussian filtering concept. However, the particle location information is considered in the DBS method with a different implementation from the DD method.

5.2. Choice of heat transfer coefficient models

In the forced convection case studied here, besides the coupling methods, the heat transfer correlation has a critical influence on the results. The Nu number calculated by the two correlations, which is mentioned in Section 2.2.2 for the fixed bed discussed above, is plotted together with the experimental fitting in Fig. 15.

Because the bed is packed in a simple cubic configuration, the bed voidage is relatively higher than the one in random packing, and there are unobstructed tunnels for the gas phase to flow. Hence, the bed correlations will overestimate the heat transfer coefficient, even though bed voidage is already considered in equation [4], and since the correlations are obtained for randomly packed beds.

Predicted results of both gas phase and solid phase temperatures, using the two different correlations of the heat transfer coefficients with the DBS method, are shown in Fig. 16. The larger the calculated coefficient, the higher heat transfer rate is predicted, which means a higher gas phase temperature at the outlet in the beginning of the simulation. Correspondingly, the solid phase temperature was under-predicted, as shown in Fig. 16(b). Compared to using the correlations, the heat transfer coefficient obtained by experimental fitting predicted results that are in better agreement with the experimental measurement. It shows that the newly developed coupling method improved the accuracy of the simulation.

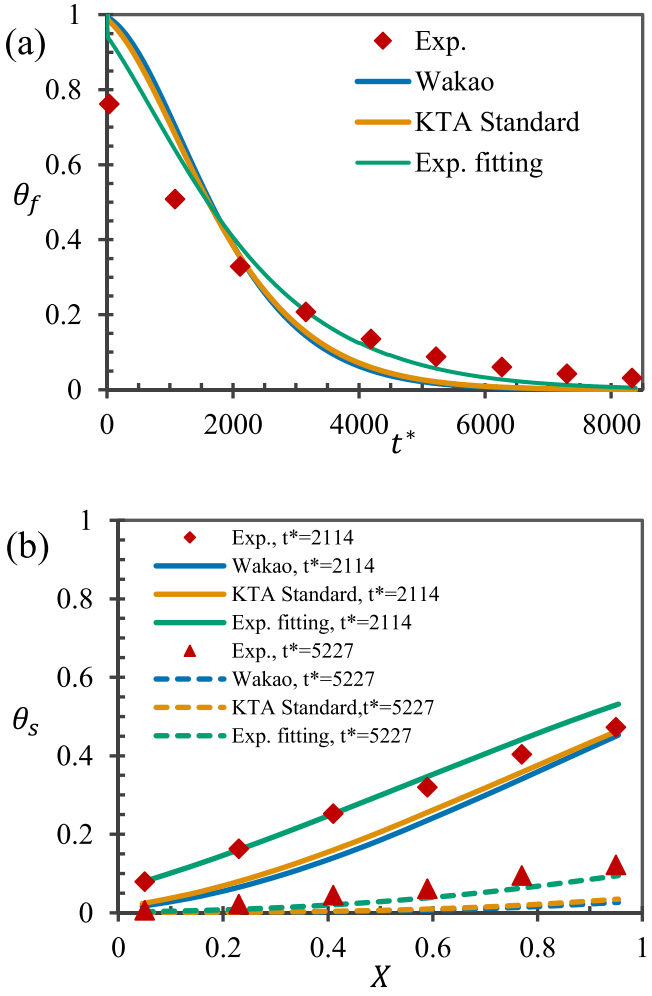

Fig. 16. Comparisons of experimental and predicted temperatures of gas and solid phases with different convection heat transfer coefficients: (a) gas phase outlet temperature θ_f; (b) solid phase temperature θ_s.

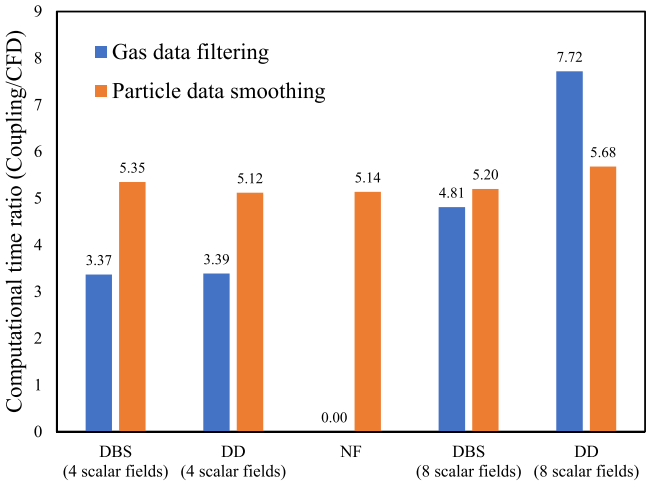

Fig. 17. Computational cost comparisons of different coupling methods.

5.3. Statistics of the computational cost

The computational cost of different coupling methods is studied in this section. The computational cost can be divided into four parts: cost of solving the gas phase governing equations, cost of solving the DEM, cost induced by the smoothing method and cost induced by the gas phase filtering. In all the simulations, a grid with 10,692 cells is employed, and the CPU time spent on solving the gas phase governing equations is used as a reference for each case. The most expensive part of the simulations is associated with solving the DEM model. A moderate number of 396 steel sphere particles were described by the DEM, yet it required about 10 times as much the cost associated with solving the gas phase governing equations. For different coupling methods, the smoothing and filtering costs are shown in Fig. 17 as ratios to the cost of resolving the gas phase. There are three variables for the particle smoothing method (the particle volume, S_m and S_h) that need to be smeared. The source term has two coefficients with an implicit implementation, and one of the coefficients of the momentum source term is a vector field. Hence there are an equivalent of 7 scalar fields that the diffusion operator needs to be applied to. As shown in Fig. 17, the cost of the diffusion-based smoothing is similar in different cases and is about 5 times the cost of resolving the gas phase governing equations.

For the gas filtering, there are two fields ($\mathbf{U}_f$ and T_f) that need to be filtered, which are equivalent to 4 scalar fields. However, the number of the filtered gas property fields could be extended if other thermal property fields or even the species concentration fields need to be smoothed, e.g., in a combustion simulation of solid fuel. As a test case, 4 additional fields were added, which are: ρ_f, μ_f (viscosity), k_f (thermal conductivity) and c_{pf} (heat capacity), and the statics of the filtering with more quantities (the complete set of 6 fields) are also shown in Fig. 17. The DBS method only requires the diffusion operation once, and the rest of the calculation is mainly looping the mesh faces. For fewer filtered quantities, the DBS method requires almost the same computational cost as the DD method, while for more quantities it is shown to represent significant savings compared to the DD method, simply because face looping is faster than solving matrices.

It is worth mentioning that there is much room for optimizing the computational cost of the coupling method. The main factor that influences the computational cost is the diffusion time step τ. In the current settings, the total steps from 0 to τ are 6, while fewer time steps, for example 3, could be applied [29]. For the diffusion of the S field with the explicit method, much smaller time steps are however required at the beginning, and in this work 25 adjusted time steps are applied. This could be further optimized to enhance computational efficiency. In general, it is shown that the developed coupling method is affordable and efficient in the CFD-DEM simulations.

6. Conclusion

A novel coupling method for multi-phase gas-solid simulations under the CFD-DEM framework is developed. The method is designed for the simulation with large-sized particles and a sub-particle scale mesh. The coupling includes both smoothing the particle point data and filtering the gas field data. The smoothing is based on a newly proposed diffusion-based smoothing, and filtering is also based on the diffusion operation. The coupling algorithm is validated using a simulation of air cooling steel sphere by forced convection in a fixed bed, which is in a well-defined cubic packing configuration. The overall heat transfer rate is well predicted. Compared to coupling methods only considering the smoothing, the newly developed approach, including the filtering method, has a better performance in reducing the particle's disturbance of the flow field. The method converges even at a small characteristic length of the coupling method.

The new filtering method developed in the coupling algorithm is able to reconstruct the particle ambient quantities of the gas phase, even at a computational size much smaller than the particle diameter. The DBS method can calculate the averaged gas phase quantities based on the particle location and size without a computationally costly search algorithm. The filtered quantities are directly reconstructed at the cell of the particle's centroid, simplifying the coupling scheme and as well as the implementation into the CFD solver. The DBS method is also shown to be computationally efficient and well suited for implementation in parallel computing. In this study, only the simulations of fixed beds in dense packing were conducted; however, for other regimes, for example, the dilute granular flow, the behavior of the new coupling method, and the choosing of the coupling parameters need to be further investigated.

Declaration of Competing Interest

The authors declare that they have no known competing financial interests or personal relationships that could have appeared to influence the work reported in this paper.

CRediT authorship contribution statement

Jingyuan Zhang: Conceptualization, Methodology, Software, Data curation, Writing – original draft. **Tian Li:** Conceptualization, Software, Writing – review & editing. **Henrik Ström:** Writing – review & editing. **Boyao Wang:** Methodology, Writing – review & editing. **Terese Løvås:** Supervision, Writing – review & editing.

Data availability

Data will be made available on request.

Acknowledgments

The authors acknowledge support from the Research Council of Norway and a number of industrial partners through the project BioCarbUp (294679) and Project GrateCFD (267957). NTNU IDUN/EPIC computing cluster provided high-performance computational resources for CFD simulations. Henrik Ström gratefully acknowledges co-financing from the Centre for Combustion Science and Technology (CECOST) and the Swedish Gasification Centre (SFC).

Appendix A

For a gas phase field (e.g. the temperature field T) the weights field S is based on the particle location, and $\Sigma S = 1$. For the initial S field, the value of the cells only where the particle's centroid locates is 1, otherwise is 0. Start with the diffusion equation of the weights field S:

$$\frac{\partial S}{\partial \tau} - D\nabla^2 S = 0, \tag{A.1}$$

where D is the diffusivity. The weights field S will be in Gaussian distribution. The implicit form of discretization of the equation is shown as follows:

$$\frac{S^{n+1} - S^n}{\delta \tau} - D(\nabla^2 S)^{n+1} = 0, \tag{A.2}$$

which is equivalent to:

$$AS^{n+1} = b, \tag{A.3}$$

where A contains the discretization parameters for the time step $n+1$ and b contains the discretization parameters of the time step n. b has a form of:

$$b = BS^n. \tag{A.4}$$

The linear system can therefore be rewritten as:

$$AS^{n+1} = BS^n. \tag{A.5}$$

It should be mentioned that the matrix A is a symmetric matrix and matrix B is a diagonal matrix. After the diffusion of the weights field S, the weighted temperature T can be calculated as $(S^n)^T T^0$. Directly applying the same diffusion operation for field T from T^0 to T^n, the targeted weighted average should be $(S^0)^T T^n$. The following derivation is going to prove that $(S^n)^T T^0$ is equivalent to $(S^0)^T T^n$

With a same diffusivity D, the diffusion equation of the T field is:

$$\frac{\partial T}{\partial t} - D\nabla^2 T = 0, \tag{A.6}$$

which can be represented as the following linear system:

$$AT^{n+1} = BT^n. \tag{A.7}$$

If the mesh, time step, and diffusivity are the same, the coefficients A and B will be the same for the diffusion of S and T. The superscript T means the transpose of the vector. Expand the S^n and T^n, $(S^n)^T T^0$ becomes:

$$\left(\prod_{i=1}^{n} A^{-1}BS^0\right)^T T^0 = (S^0)^T \left(\prod_{i=1}^{n} A^{-1}B\right)^T T^0, \tag{A.8}$$

and $(S^0)^T T^n$ becomes:

$$(S^0)^T \left(\prod_{i=1}^{n} A^{-1}B\right) T^0 \tag{A.9}$$

To prove that $(S^n)^T T^0 = (S^0)^T T^n$, is equal to prove:

$$\left(\prod_{i=1}^{n} A^{-1}B\right)^T = \prod_{i=1}^{n} A^{-1}B \tag{A.10}$$

Expand the term $(\prod_{i=1}^{n} A^{-1}B)^T$, and considering that the matrix A is a symmetric matrix and matrix B is a diagonal matrix:

$$\begin{aligned}\left(\prod_{i=1}^{n} A^{-1}B\right)^T &= \prod_{i=1}^{n} (A^{-1}B)^T = \prod_{i=1}^{n} B^T (A^{-1})^T = \prod_{i=1}^{n} B(A^T)^{-1} \\ &= \prod_{i=1}^{n} BA^{-1} = \prod_{i=1}^{n} A^{-1}B\end{aligned} \tag{A.11}$$

It proves that if the diffusion operation is directly applied to the T field, then, $T^n(\mathbf{x}) = \int T^0(\mathbf{y}) g(|\mathbf{x} - \mathbf{y}|) d\mathbf{y}$, where g is a Gaussian kernel.

References

[1] H. Wu, N. Gui, X. Yang, J. Tu, S. Jiang, A smoothed void fraction method for CFD-DEM simulation of packed pebble beds with particle thermal radiation, Int. J. Heat Mass Transf. 118 (2018) 275–288.
[2] H. Salman, M. Soteriou, Lagrangian simulation of evaporating droplet sprays, Phys. Fluids 16 (2004) 4601–4622.
[3] K. Cheng, Y. Wang, Q. Yang, A semi-resolved CFD-DEM model for seepage-induced fine particle migration in gap-graded soils, Comput. Geotech. 100 (2018) 30–51.
[4] J. Yang, Q. Wang, M. Zeng, A. Nakayama, Computational study of forced convective heat transfer in structured packed beds with spherical or ellipsoidal particles, Chem. Eng. Sci. 65 (2010) 726–738.
[5] D. Jajcevic, E. Siegmann, C. Radeke, J. Khinast, Large-scale CFD–DEM simulations of fluidized granular systems, Chem. Eng. Sci. 98 (2013) 298–310.
[6] J. Capecelatro, O. Desjardins, An Euler–Lagrange strategy for simulating particle-laden flows, J. Comput. Phys. 238 (2013) 1–31.
[7] J. Zhang, T. Li, H. Ström, T. Løvås, Computationally efficient coarse-graining XDEM/CFD modeling of fixed-bed combustion of biomass, Combust. Flame 238 (2022) 111876.

[8] J. Wiese, F. Wissing, D. Höhner, S. Wirtz, V. Scherer, U. Ley, H. Behr, DEM/CFD modeling of the fuel conversion in a pellet stove, Fuel Process. Technol. 152 (2016) 223–239.
[9] S. Wang, Y. Shen, CFD-DEM study of biomass gasification in a fluidized bed reactor: effects of key operating parameters, Renew. Energy 159 (2020) 1146–1164.
[10] X. Ku, T. Li, T. Løvås, CFD–DEM simulation of biomass gasification with steam in a fluidized bed reactor, Chem. Eng. Sci. 122 (2015) 270–283.
[11] Z. Peng, E. Doroodchi, C. Luo, B. Moghtaderi, Influence of void fraction calculation on fidelity of CFD-DEM simulation of gas-solid bubbling fluidized beds, AIChE J. 60 (2014) 2000–2018.
[12] S. Balachandar, K. Liu, M. Lakhote, Self-induced velocity correction for improved drag estimation in euler–lagrange point-particle simulations, J. Comput. Phys. 376 (2019) 160–185.
[13] K. Liu, M. Lakhote, S. Balachandar, Self-induced temperature correction for inter-phase heat transfer in euler-lagrange point-particle simulation, J. Comput. Phys. 396 (2019) 596–615.
[14] P. Gualtieri, F. Picano, G. Sardina, C. Casciola, Exact regularized point particle method for multi-phase flows in the two-way coupling regime, arXiv preprint arXiv:1405.6969(2014).
[15] P. Ireland, O. Desjardins, Improving particle drag predictions in euler–lagrange simulations with two-way coupling, J. Comput. Phys. 338 (2017) 405–430.
[16] J. Johansen, P. Jensen, P. Glarborg, M. Mancini, R. Weber, R. Mitchell, Extension of apparent devolatilization kinetics from thermally thin to thermally thick particles in zero dimensions for woody biomass, Energy 95 (2016) 279–290.
[17] L. Wang, J. Ouyang, C. Jiang, Direct calculation of voidage in the fine-grid CFD—DEM simulation of fluidized beds with large particles, Particuology 40 (2018) 23–33.
[18] B. Freireich, M. Kodam, C. Wassgren, An exact method for determining local solid fractions in discrete element method simulations, AIChE J. 56 (2010) 3036–3048.
[19] B. Glasser, I. Goldhirsch, Scale dependence, correlations, and fluctuations of stresses in rapid granular flows, Phys. Fluids 13 (2001) 407–420.
[20] J. Zhang, T. Li, H. Ström, T. Løvås, Grid-independent Eulerian-Lagrangian approaches for simulations of solid fuel particle combustion, Chem. Eng. J. 387 (2020) 123964.
[21] C. Fernandes, D. Semyonov, L. Ferrás, J. Nóbrega, Validation of the CFD-DPM solver DPMFoam in openFOAM®through analytical, numerical and experimental comparisons, Granular Matter 20 (2018) 64.
[22] D. Gidaspow, Multiphase Flow and Fluidization: Continuum and Kinetic Theory Descriptions, Academic Press, 1994.
[23] R. Mehrabian, S. Zahirovic, R. Scharler, I. Obernberger, S. Kleditzsch, S. Wirtz, V. Scherer, H. Lu, L. Baxter, A CFD model for thermal conversion of thermally thick biomass particles, Fuel Process. Technol. 95 (2012) 96–108.
[24] Z. Peng, E. Doroodchi, B. Moghtaderi, Heat transfer modelling in discrete element method (DEM)-based simulations of thermal processes: theory and model development, Prog. Energy Combust. Sci. 79 (2020) 100847.
[25] H. Wu, N. Gui, X. Yang, J. Tu, S. Jiang, Parameter analysis and wall effect of radiative heat transfer for CFD-DEM simulation in nuclear packed pebble bed, Exp. Comput. Multiphase Flow 3 (2021) 250–257.
[26] G. Batchelor, R. O'brien, Thermal or electrical conduction through a granular material, Proc. R. Soc. London A Math. Phys. Sci. 355 (1977) 313–333.
[27] Z. Zhou, A. Yu, P. Zulli, Particle scale study of heat transfer in packed and bubbling fluidized beds, AIChE J. 55 (2009) 868–884.
[28] N. Wakao, S. Kagei, Heat and Mass Transfer in Packed Beds, Taylor & Francis (1982).
[29] R. Sun, H. Xiao, Diffusion-based coarse graining in hybrid continuum–discrete solvers: theoretical formulation and a priori tests, Int. J. Multiphase Flow 77 (2015) 142–157.
[30] R. Sun, H. Xiao, Diffusion-based coarse graining in hybrid continuum–discrete solvers: applications in CFD–DEM, Int. J. Multiphase Flow 72 (2015) 233–247.
[31] M. Germano, Others turbulence- the filtering approach, J. Fluid Mech. 238 (1992) 325–336.
[32] J. Yang, J. Wang, S. Bu, M. Zeng, Q. Wang, A. Nakayama, Experimental analysis of forced convective heat transfer in novel structured packed beds of particles, Chem. Eng. Sci. 71 (2012) 126–137.
[33] B. Wang, W. Shi, Z. Miao, Confidence analysis of standard deviational ellipse and its extension into higher dimensional euclidean space, PLoS ONE 10 (2015). e0118537